Translational spectroscopy studies of the photodissociation dynamics of O_4^-

C. R. Sherwood, K. A. Hanold, M. C. Garner, K. M. Strong, and R. E. Continetti
Department of Chemistry and Biochemistry, University of California, San Diego, 9500 Gilman Drive, La Jolla, California 92093-0314

(Received 16 April 1996; accepted 17 September 1996)

An investigation of the photodissociation dynamics of the dimer anion O_4^- at 523.6, 349.0, and 261.8 nm is reported. Product translational energy and angular distributions have been obtained using photofragment translational spectroscopy in a fast ion beam. At all wavelengths photodissociation $(O_4^- + h\nu \rightarrow O_2 + O_2^-)$ is observed to proceed via a rapid parallel electronic transition, with the photofragment angular distribution strongly peaked along the laser electric vector. The lowest energy photodissociation channel produces $O_2(a^1\Delta_g)$ and ground state $O_2^-(X^2\Pi_g)$, indicating that O_4^- is a doublet anion. The partitioning of energy in the dissociation reveals a complicated wavelength dependence. © *1996 American Institute of Physics.* [S0021-9606(96)00548-X]

I. INTRODUCTION

Interest in the study of photodestruction dynamics in cluster ions has grown due to the central role they may play in developing an understanding of the transition from the photochemistry of isolated molecules to condensed phases.[1] Homogeneous cluster ions, however, can exhibit bonding interactions distinct from either isolated molecules or extended condensed phase systems.[2] Dimer anions present especially interesting systems for study, since the excess electron may be either localized or delocalized depending on the nature of the charge-transfer interaction between the monomers.[3,4] Studies of the dynamics of photodestruction, *via* both photodetachment and photodissociation, provide an important test of our understanding of the structure and bonding of dimer anions. The present work describes studies of the photodissociation dynamics of the tetroxide ion, O_4^-, at 523.6, 349.0, and 261.8 nm.

The photodestruction of O_4^- has been studied in a series of photodestruction cross-section measurements.[5–8] Total cross sections measured in the 400- to 800-nm range showed no resolvable structure, and thus no evidence for long-lived excited states of the anion.[6–9] Smith *et al.* determined the threshold for the photodestruction of O_4^- to be 1.57 eV.[8] Lee and Smith[9] recognized that the photodestruction of O_4^- was likely to proceed by both photodissociation [Eq. (1)] and dissociative photodetachment [Eq. (2)],

$$O_4^- + h\nu \rightarrow O_2 + O_2^-, \tag{1}$$

$$O_4^- + h\nu \rightarrow O_2 + O_2 + e^-. \tag{2}$$

Early mass spectrometric work by Conway and Nesbitt indicated that O_4^- is stable with respect to dissociation into $O_2 + O_2^-$ by 0.59 eV.[10] More recent mass spectrometric measurements by Hiraoka indicate a stability of 0.46 ± 0.02 eV.[11]

Johnson and co-workers studied the photodissociation of O_4^- using photoelectron spectroscopy.[12–14] Photoelectron spectra reported at 532 and 355 nm showed no resolved vibrational structure. In the O_4^- photoelectron spectrum, Johnson and co-workers also observed the weak features of the photoelectron spectrum of O_2^-.[15] A study of the laser-power dependence showed that this signal originated from photodissociation of O_4^- [Eq. (1)], followed by photodetachment of nascent O_2^- by a second photon.[13,16] In a recent study of the dynamics of the dissociative photodetachment [Eq. (2)] of O_4^- at 523.6 nm[17–19] we have also observed photodissociation of O_4^-.

Experimental studies on the structure of O_4^- have employed matrix-isolation techniques.[20–22] These investigations have indicated a symmetric, electron-delocalized *trans*-C_{2h} structure. Theoretical calculations of the structure and energetics of O_4^- have produced a range of predicted bond energies and structures. A semiempirical self-consistent field (SCF) calculation by Conway[23] predicted a C_{2h} structure with an O–O–O bond angle of 110° and a bond energy of ~0.4 eV. The $O_2^- - O_2$ separation was found to be 2.1 Å. Ohta and Morokuma examined the structure of quartet states of O_4^- using *ab initio* techniques (unrestricted Hartree–Fock (UHF) SCF, 3-21G basis set).[24] The bond energy of 0.12 eV given by these calculations is not consistent with the observed stability of O_4^-. Li *et al.*[25] recently extended these studies of quartet states with a UHF-SCF calculation using a $6\text{-}31G+sp$ basis set and found two C_{2v} minima bound by ≈0.57 eV. These structures are well described as $O_2^- \cdot O_2$, with a separation of ≈3.2 Å. High-level converged calculations of the doublet states of O_4^- remain to be done.

In the following section, the photofragment translational spectrometer used in these studies is described. This is followed by a review of the data analysis and a presentation of the raw data. Center-of-mass translational energy and angular distributions are then presented, with an emphasis on the photodissociation channel producing $O_2^- + O_2$. The dissociation dynamics are discussed in the context of simple impulsive and Franck–Condon models for the partitioning of energy.

II. EXPERIMENT

In the experiments presented in this paper, both molecular products from a photodissociation event are measured in

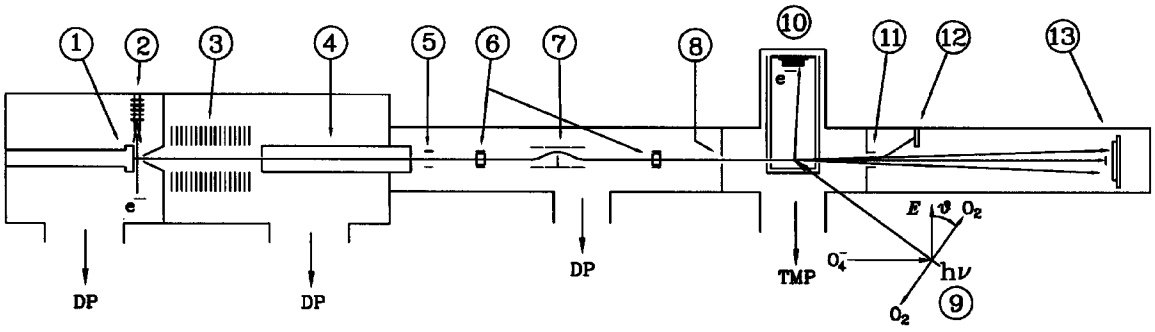

FIG. 1. Schematic of the apparatus. The photoelectron spectrometer, (10), is not used in the present experiments. The laser electric vector, **E**, is shown vertically polarized relative to the ion beam direction. The polar angle (θ) of photofragment recoil relative to the **E** vector is also shown. The chamber is differentially pumped by diffusion pumps (DP) and a turbomolecular pump (TMP).

coincidence with a photofragment translational spectrometer. This allows the measurement of kinetic energy and angular distributions characterizing photodissociation and dissociative photodetachment processes. A schematic of the apparatus is shown in Fig. 1. The apparatus consists of a mass-selected anion source, a photoelectron spectrometer,[26] and a photofragment translational spectrometer capable of detecting neutrals or anions. A brief description of photofragmentation studies with this apparatus has been previously published.[27]

The fast-beam photofragment translational spectrometer is similar to that used by Neumark and co-workers to study the photodissociation of neutral-free radicals.[28] O_4^- is generated by crossing a pulsed supersonic expansion of neat O_2 (1) with a 1-keV electron beam (2).[29] The nascent anions cool in the expansion and pass through a skimmer into a differentially pumped chamber where they are accelerated to a beam energy of 2.5–7 keV (3). After acceleration, the ion beam is referenced to ground potential using a potential switch (4).[13] Anions are separated according to mass by a time-of-flight technique that involves a rapidly switched potential perpendicular to the beam axis (5) and a small entrance aperture (8) into the laser-interaction region.[30] Electrostatic deflectors (6) are employed to direct the ion beam through the entrance aperture. Ions are also guided over a beam-block situated on the beam axis[31] (7) which removes fast neutral particles from the beam.

Anions at the mass of interest are intersected at a right angle by a linearly polarized laser pulse (9) from the frequency doubled (523.6 nm), tripled (349.0 nm), or quadrupled (261.8 nm) output of a Nd:YLF laser (Spectra Physics TFR). The laser yields 200 μJ at 523.6 nm and 20–30 μJ at either of the ultraviolet wavelengths using appropriate nonlinear optics. The laser pulse is 6 ns long full-width-at-half-maximum (FWHM) and is focused to a 0.5-mm-diam spot at the point of ion–laser interaction. Absorption of a photon by O_4^- leads to either photodissociation producing a neutral and an ionic photofragment or dissociative photodetachment producing two neutral photofragments and a photoelectron.

Photofragments recoil out of the beam over a 96-cm flight path toward a two-particle time- and position-sensitive detector (13). Fragments must clear a 7-mm-wide horizontal beam stop to impinge on the detector microchannel plates. The beam stop is centered on the ion-beam axis to prevent undissociated ions from reaching the detector. A double wedge-and-strip anode encodes the position of incident photofragments on each half of the detector.[28] The face of the detector is held at ground potential to enable the detection of both neutral and charged products. Due to the one-particle-per-shot detection limit and the coincidence nature of the experiment, the photodestruction rate is limited to much less than one event per laser shot. To speed data acquisition the ion source and laser system are operated at a repetition rate of 500 Hz. The experimental coincidence count rate is $\approx$20 Hz.

Using the time- and position-of-arrival information it can be determined if the two photofragments originated in a single dissociation event by checking for conservation of momentum given the possible dissociation pathways. Once the mass of the photofragments is determined, the kinetic energy and recoil angle of the photofragments are calculated, with the results histogrammed in a raw translational energy and angular distribution, $N(E_T,\theta)$.[28,32] The photofragment translational spectrometer has been calibrated using the photodissociation of O_2^- by the $A \leftarrow X$ transition[33] at 261.8 nm. This calibration showed that energy resolution is no worse than $\Delta E/E \sim 10\%$.

The photofragment translational spectrometer is operated using two different collection modes. Either neutral *and* ionic photofragments are simultaneously collected ($N+I$) or *only* neutral photofragments are collected (N-only). If the N-only mode is selected, then the deflection field (11) is used to direct undissociated ions and ionic photofragments to a detector (12) to measure the ion beam intensity. In the $N+I$ mode, the deflection field and detector are not used and undissociated ions are dumped into the beam stop on the front of the photofragment detector. Comparison of coincidence data taken in the two modes allows spectral signatures due to photodissociation to be distinguished from dissociative photodetachment.

III. DATA ANALYSIS

The use of a large-area detector permits a wide kinematic range of photofragments to be detected in coincidence, allowing the simultaneous and correlated measurement of photofragment energy and angular distributions in a single experiment. The beam stop and finite detector size, however, can discriminate against certain portions of these distributions. The photofragment mass ratio, angular distributions, and laser electric vector direction all have a strong influence on this discrimination. To obtain the true form of the center-of-mass distributions, the spectra must be corrected for the incomplete detector acceptance.[28] Since the detector geometry and experimental conditions are known, it is straightforward to numerically correct for the limited acceptance and directly invert the raw data to the center-of-mass frame kinetic energy and angular distribution $P(E_T,\theta)$. We perform the detector acceptance correction following the examples of Los[34] and Neumark.[28] The corrected and normalized photofragment energy and angular distribution $P(E_T,\theta)$ is then least-squares fit to the separable form:

$$P(E_T,\theta)=P(E_T)[1+\beta(E_T)P_2(\cos\theta)]. \tag{3}$$

Here, $P_2(\cos\theta)$ is the second Legendre polynomial in $\cos\theta$, $\beta(E_T)$ is the anisotropy parameter for a given translational energy release, and $P(E_T)$ is the translational energy release distribution. $\beta(E_T)$ describes the energy dependent angular distribution, and varies between the limits of $\cos^2\theta$ ($\beta=2$, parallel transition) and $\sin^2\theta$ ($\beta=-1$, perpendicular transition) in the limit of prompt axial recoil.[35]

The preceding discussion describes the procedure used to extract $P(E_T)$ and $\beta(E_T)$ from the data recorded in a single experiment. While the detection scheme samples a wide range of E_T and θ space, the coverage is not complete. A more complete $P(E_T,\theta)$ can be determined by combining data acquired under different experimental conditions (beam energy, laser polarization and/or detector position). Due to the large kinematic range of each data set, it is straightforward to scale different data sets and combine them. Adding these data sets together allows not only more complete distributions to be obtained but also establishes confidence levels for the $P(E_T)$ and $\beta(E_T)$ distributions.[36] The $P(E_T)$ and $\beta(E_T)$ distributions reported in this paper were obtained in this manner. The quality of the $P(E_T)$ and $\beta(E_T)$ found by this approach can be checked using a Monte Carlo forward convolution simulation to compare to the raw data.[28] Simulated data is generated by averaging $P(E_T)$ and $\beta(E_T)$ over apparatus parameters including the ion beam size, velocity and angular distribution, the laser beam spot size, detector geometry and the time- and position-resolution of the detector.

IV. RESULTS—PHOTODISSOCIATION OF O_4^- AT 523.6, 349.0, AND 261.8 nm

Raw photofragment translational energy release spectra, $N(E_T)$, from the photodestruction of O_4^- at 523.6 nm (2.368 eV), 349.0 nm (3.552 eV), and 261.8 nm (4.736 eV) are presented in Fig. 2. These spectra were recorded with a beam energy of 4 keV and the electric vector of the laser polarized along the ion-beam direction (horizontal polarization). The solid curves in each spectrum were obtained from detection of both coincident neutral–neutral and anion–neutral pairs ($N+I$ mode), while the dotted lines correspond to neutral–neutral coincidences only (N-only mode). The differences in the spectra indicate that both photodissociation [Eq. (1)] and dissociative photodetachment [Eq. (2)] occur at each wavelength. Only equal-mass photofragment pairs were observed. Analysis of data taken under a variety of beam energies and detector positions showed no evidence for other primary product channels such as O_3+O or stable O_4 after photodetachment.

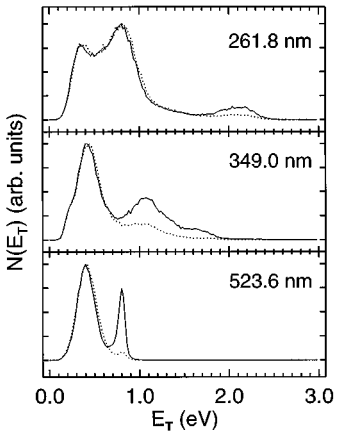

FIG. 2. Wavelength-dependent raw translational energy release $N(E_T)$ spectra for the photodestruction of O_4^- at a beam energy of 4 keV. The data were recorded with the laser polarized along the ion beam. The solid lines corresponds to ion+neutral ($N+I$) coincidences. The dotted lines correspond to coincident neutrals only (N-only).

A. 523.6-nm translational energy release spectra

The spectrum at 523.6 nm in the bottom frame of Fig. 2 shows two features in both the $N+I$ and N-only spectra. The broad peak at 0.40 eV is present in both spectra while the smaller, narrower peak at 0.80 eV is reduced in the N-only

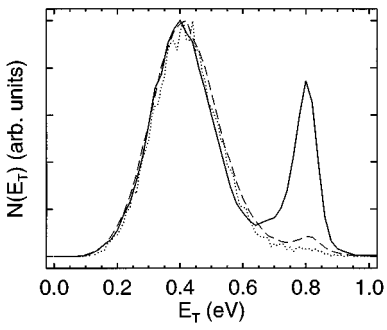

FIG. 3. The dependence of the photodissociation peak at $E_T=0.80$ eV in the raw 523.6-nm data on fragment collection mode and laser power is shown. Solid line: ($N+I$), high laser power; dashed line (N-only), high laser power; dotted line (N-only), laser power reduced by a factor of 10. The energy shifts in the three spectra indicate a precision of $\approx\pm0.02$ eV in translational energy measurements.

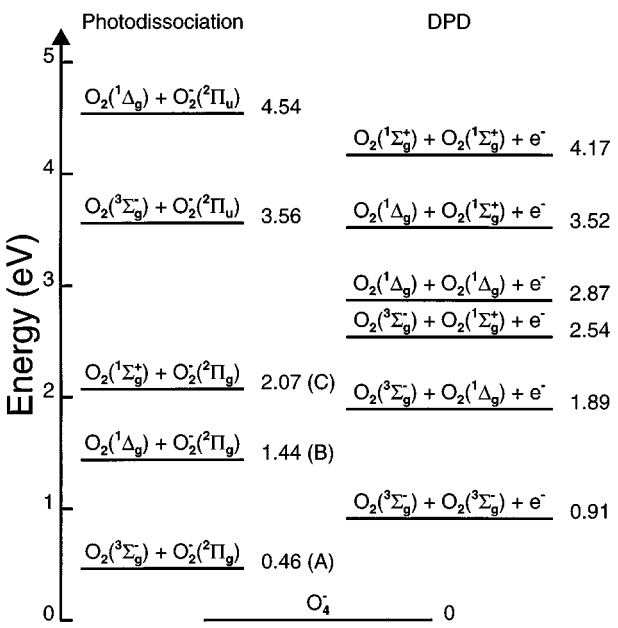

FIG. 4. Energetics diagram for photodissociation and dissociative photodetachment thresholds in O_4^-. The photodissociation channels labeled B and C are observed to occur. The dissociative photodetachment thresholds correspond to the production of a zero kinetic energy electron.

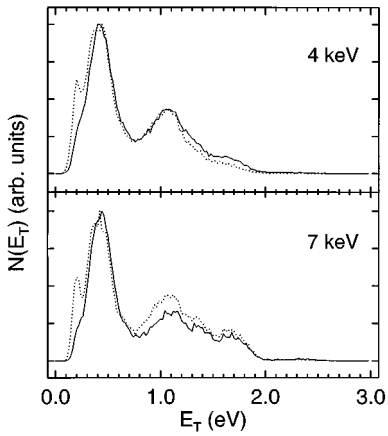

FIG. 5. Raw $N(E_T)$ spectra in the $(N+I)$ mode at 349.0 nm. The solid and dotted lines represent data taken with horizontal and vertical laser polarization, respectively. The upper and lower frames show the effect of beam energy on the form of the spectra.

spectrum. The 0.80-eV peak in the N-only spectrum is found to be laser power dependent and is assigned to photodissociation. The power dependence studies, shown in Fig. 3, indicate that the O_2^- fragment produced in photodissociation is being photodetached by a second photon at higher laser powers. As discussed earlier, this effect was also observed in the photoelectron spectrum of O_4^- at 532 nm by Johnson and co-workers.[13] The broad feature at 0.40 eV obtained in both fragment collection modes is assigned to dissociative photodetachment. The photodissociation peak at 0.80 eV has a FWHM of only 0.09 eV.

The narrow photodissociation peak allows an independent determination of the O_4^- bond energy with respect to O_2^- and O_2. Neglecting internal energy in the parent O_4^- and internal excitation in the O_2^- and O_2 products, the maximum translational energy release in photodissociation is given by the difference between the photon energy and the $O_2^- - O_2$ bond dissociation energy. Using the bond energy determined by Hiraoka (0.46 eV),[11] ground state O_2^- and O_2 products would be expected to have translational energy releases up to 1.91 eV. The narrow photodissociation peak rising below 1.0 eV thus indicates that excited $O_2(a^1\Delta_g)$ and ground state $O_2^-(X^2\Pi_g)$ are the lowest energy products of photodissociation at this wavelength. Assigning $E_{T,\max} = 1.00 \pm 0.02$ eV as the maximum translational energy, the bond energy for the production of ground-state O_2^- and O_2 is redetermined at $D_0 = 0.39 \pm 0.02$ eV. This value ignores the possibility of internal excitation in the O_4^- parent yielding products at higher translational energies. Given that no good diagnostic exists for the measurement of parent internal energy, Hiraoka's value for the bond energy is adopted, yielding $E_{T,\max} = 0.93 \pm 0.02$ eV. This bond energy, in conjunction with spectroscopic data for O_2 and O_2^-,[37,38] determines the energetics for the possible photodestruction channels of O_4^- as shown in Fig. 4. Since the dissociation of a quartet state into a singlet and doublet is spin-forbidden,[39] the result also indicates that the O_4^- ground state is likely to be a doublet.

B. 349.0-nm translational energy release spectra

Translational energy release spectra obtained at 349.0 nm are shown in the middle frame of Fig. 2. The complexity of these spectra indicate that new dissociation pathways are accessed at this wavelength. The dominant feature appears at 0.43 eV in both the $N+I$ and N-only spectra and is assigned to dissociative photodetachment. There is also a peak at 1.05 eV and a shoulder centered at ~1.65 eV that are reduced in the N-only spectrum. These two features are assigned to photodissociation. Unlike the 523.6-nm data, however, reduction of the laser power by a factor of 3 causes no change in the N-only spectrum. This is in large part due to the fact that the maximum laser fluences available at both 349.0 and 261.8 nm are only $\approx$4 MW/cm^2 vs 25 MW/cm^2 at 523.6 nm. The N-only signal at high energies can be attributed to either rapid autodetachment of vibrationally excited O_2^- produced in photodissociation or an overlapping dissociative photodetachment channel. Due to the low electron affinity of O_2, autodetachment of $O_2^-(X^2\Pi_g)$ occurs for vibrational states $v>3$ on a time scale of <100 ps,[40] much shorter than the time-of-flight to the ion deflection field (~1–4 μs).

Due to the detector acceptance, the raw spectra in Fig. 2 do not reveal all important features of the translational energy release distribution for 349.0 nm. Spectra recorded with beam energies of 4 and 7 keV and different laser polarizations are shown for $N+I$ data in Fig. 5. These spectra reveal two features not evident in the spectrum in Fig. 2, which was recorded with a horizontal laser polarization and a beam energy of 4 keV. A sharp peak at 0.2 eV appears at low beam energies, preferentially when the laser is vertically polarized.

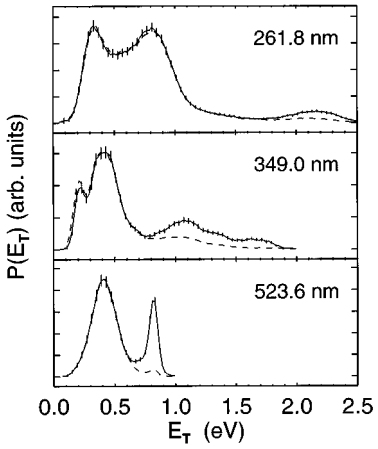

FIG. 6. $P(E_T)$ distributions in the $(N+I)$ mode (solid line) and (N-only) mode (dashed line) at 523.6, 349.0, and 261.8 nm. Error bars ($\pm 2\sigma$) are shown for the $(N+I)$ data.

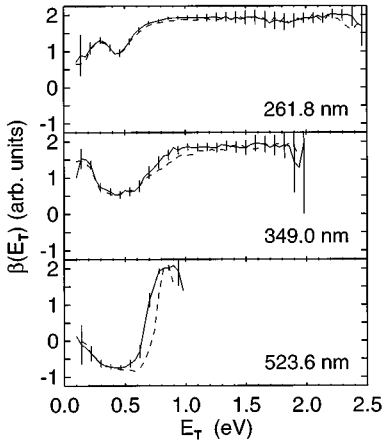

FIG. 7. $\beta(E_T)$ distributions in the $(N+I)$ mode (solid line) and (N-only) mode (dashed line) at 523.6, 349.0, and 261.8 nm. Error bars ($\pm 2\sigma$) are shown for the $(N+I)$ data.

This peak shows no collection-mode dependence and is assigned to dissociative photodetachment. A shoulder at ~1.32 eV is also more evident in the spectra in Fig. 5 indicating another photodissociation pathway. Product state assignments for these photodissociation features are inferred from the energy level diagram in Fig. 4. The highest translational energy products appear 0.2 eV below the threshold for $O_2(a^1\Delta_g)+O_2^-(X^2\Pi_g)$ and the shoulder at ~1.32 eV is immediately below the threshold for production of $O_2(b^1\Sigma_g^+)+O_2^-(X^2\Pi_g)$.

C. 261.8-nm translational energy release spectra

The translational energy release spectra at 261.8 nm are simpler and contain three main features (top frame, Fig. 2). The dominant features are a large peak at 0.80 eV and a prominent shoulder at ~0.35 eV present in both $N+I$ and N-only spectra. These features are assigned to dissociative photodetachment. A broad feature from 1.8–2.5 eV is reduced in the N-only spectrum and is assigned to photodissociation. The photodissociation feature exhibits no power dependence in the N-only spectra, as observed in the 349.0-nm experiment. Once again, autodetachment of vibrationally excited O_2^- can explain the presence of the photodissociation feature in the neutrals-only spectrum. Examination of the energy level diagram indicates that the observed onset of the photodissociation feature at ~2.5 is 0.2 eV less than the maximum E_T expected for dissociation into $O_2(b^1\Sigma_g^+)+O_2^-(X^2\Pi_g)$.

D. Center-of-mass energy and angular distributions

Using the procedures discussed in Sec. III to correct for the detector acceptance, the distributions $P(E_T)$ and $\beta(E_T)$ are determined for each wavelength. These distributions for both the $N+I$ and N-only modes are shown in Figs. 6 and 7, respectively. The similarity of the $P(E_T)$ to the raw data show that for dissociation into equal mass fragments with the angular distributions exhibited by O_4^-, the detector acceptance has only a small effect on the data. In overview, both $P(E_T)$ and $\beta(E_T)$ exhibit a large wavelength dependence. While $P(E_T)$ are different for $N+I$ and N-only data, $\beta(E_T)$ is similar for the two collection modes. The similarity in the angular distributions for both modes confirms the importance of photodissociation followed by autodetachment leading to the signal seen at high translational energies in the N-only data at 349.0 and 261.8 nm. Assuming that the ranges of E_T corresponding to photodissociation and dissociative photodetachment do not significantly overlap, an integrated branching ratio (dissociative photodetachment/photodissociation) can be calculated from the $N+I$ $P(E_T)$'s at each wavelength. The branching ratio at 523.6 nm, assuming all data below 0.65 eV is attributable to dissociative photodetachment and all above 0.65 eV is from photodissociation is 3 ± 0.5:1. At 349.0 and 261.8 nm, the dividing points are 0.80 eV and 1.6 eV, respectively, and the branching ratios are 2 ± 0.5:1 and 10 ± 2:1, respectively. The error bars are determined by recalculating the branching ratios after moving the dividing points ± 0.1 eV at 523.6 and 349.0 nm, and ± 0.2 eV at 261.8 nm. At the highest photon energy, optical excitation to the photodetachment continuum is significantly favored over the ionic photodissociation continuum.

At 523.6 nm, the $\beta(E_T)$ shown in Fig. 7 exhibits dramatic variation over the translational energy range. For the dissociative photodetachment feature peaking at 0.40 eV in the $P(E_T)$, the angular distribution is characterized by $\beta \sim -0.8$, indicating that the transition moment is perpendicular to the breaking bond. $\beta(E_T)$ rises rapidly at $E_T > 0.6$ eV to $\beta \sim 1.9$, indicating that the transition moment is parallel to the bond broken in photodissociation and that prompt axial recoil is occurring. In the 349.0 nm $\beta(E_T)$ distribution at $E_T > 1.0$ eV, where photodissociation producing stable O_2^- and O_2 is known to occur, β approaches the limiting value of 2.0. This once again shows that photodissociation is prompt, with the transition moment lying along the dissociating bond. The angular distribution for the dissociative photodetachment peak at 0.43 eV is slightly parallel ($\beta \sim 0.6$), while that

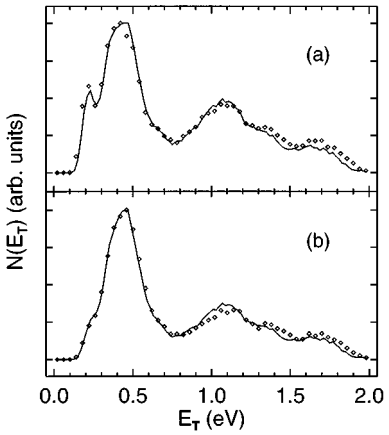

FIG. 8. Comparison of raw $N(E_T)$ spectra (points) and Monte Carlo simulation results (solid lines) for the 349.0 nm $(N+I)$-mode data recorded at a beam energy of 7 keV. Frames (a) and (b) correspond to vertical and horizontal laser polarizations, respectively.

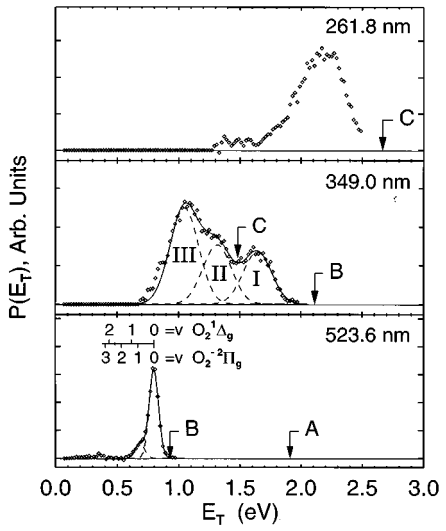

FIG. 9. Photodissociation $P(E_T)$'s given by the difference of the $(N+I)$ mode and $(N$-only) mode $P(E_T)$'s. Bottom frame: 523.6-nm data, A and B mark $E_{T,\max}$ for the accessible photodissociation channels shown in Fig. 4. The accessible product vibrational states of O_2 and O_2^- are shown by the combs. Middle frame: 349.0-nm data, B and C mark $E_{T,\max}$ for the photodissociation channels as in the bottom frame. The three components labeled I, II, and III are discussed in the text. Top frame: 261.8-nm data with $E_{T,\max}$ for photodissociation channel C.

at 0.2 eV is much more parallel ($\beta\sim1.2$). This observation supports the hypothesis of at least two dissociative photodetachment channels at this wavelength. At 261.8 nm, the photofragment angular distribution shows a parallel transition is operative throughout the range of E_T. The peak at 0.35 eV is characterized by $\beta\sim1.4$, while all data at $E_T>0.8$ eV has $\beta\sim1.9$. The 261.8 nm $P(E_T)$ and $\beta(E_T)$ are truncated at 2.5 eV due to a lack of sufficient data for determination of $\beta(E_T)$ at higher energies. The basic conclusion is that *all* photodissociation features in the data at the three wavelengths result from a parallel transition.

In order to ensure that the extracted $P(E_T)$ and $\beta(E_T)$ distributions at the three wavelengths are correct these distributions are used as input to simulations for experiments done at different beam energies and laser polarizations. If the two distributions are accurate, then the simulations should reproduce the data obtained under all different experimental conditions. Since the angular distributions for O_4^- are highly anisotropic, simulations of the translational energy release spectra recorded with horizontal and vertical polarizations are an effective test of the accuracy of $P(E_T)$ and $\beta(E_T)$. Monte Carlo forward convolution simulations for $N+I$ data at 349.0 nm and both polarizations are given in Fig. 8. This data is chosen as it covers a wide range of energy and angle space. Good overall agreement is observed between the simulation and the data.

E. Photodissociation $P(E_T)$ at 523.6, 349.0, and 261.8 nm

The $P(E_T)$ distributions for the photodissociation channels producing O_2 and stable O_2^- $(v<4)$ can be seen more clearly by taking the difference of the $P(E_T)$'s obtained from the $N+I$ and N-only data, scaled to the low-energy dissociative photodetachment peaks. These photodissociation $P(E_T)$'s are shown in Fig. 9 at 523.6, 349.0, and 261.8 nm. Also shown are the maximum translational energies for the photodissociation channels shown in Fig. 4 (see caption for Fig. 9). It is evident that the photodissociation $P(E_T)$'s show strong wavelength-dependent variations in the fraction of energy appearing in translation.

The best assignment that can be made in these spectra is in the 523.6-nm data (bottom frame of Fig. 9). In this $P(E_T)$, the peak at 0.80 eV is 0.13 eV below the expected $E_{T,\max}$ = 0.93 eV (labeled B in Fig. 9) for photodissociation producing $O_2(a^1\Delta_g,\ v=0)+O_2^-(X^2\Pi_g,\ v=0)$. While this energy difference is very close to the vibrational spacing of O_2^-, it is difficult to imagine such a sharp vibrational inversion occurring. The most likely explanation is that the sum of the rotational energies of the two diatomic products peaks at 0.13 eV. As the figure shows, there is also a nearly resolved shoulder, which is consistent with production of $O_2(a^1\Delta_g,\ v=0)+O_2^-(X^2\Pi_g,\ v=1)$. Two Gaussian curves are fit to the data, representing these two product channels. The fit indicates that 86% of the products are $O_2(v=0)+O_2^-(v=0)$, with 14% in $O_2(v=0)+O_2^-(v=1)$. At 523.6 nm, there is a strong propensity for low internal excitation (both vibrational and rotational) in the $O_2(a^1\Delta_g)+O_2^-(X^2\Pi_g)$ products.

The 349.0 nm $P(E_T)$, in the middle frame of Fig. 9, shows three broad features. These are fit with three Gaussian functions. The highest energy feature, labeled ''I'', peaks at 1.65 eV. This is 0.46 eV below the maximum translational energy (B, 2.11 eV) expected for $O_2(a^1\Delta_g)+O_2^-(X^2\Pi_g)$ products, a considerably larger offset than observed at 523.6 nm. This channel is the only plausible assignment for this feature. The second feature, labeled ''II'', peaks at 1.32 eV which is 0.16 eV below the maximum translational energy (C, 1.48 eV) expected for $O_2(b^1\Sigma_g^+,\ v=0)+O_2^-(X^2\Pi_g,\ v=0)$ products. This offset is much closer to that observed in

the 523.6 nm $P(E_T)$. The third feature, labeled ''III,'' peaks at 1.05 eV which is 0.43 eV below the maximum translational energy for the $O_2(b^1\Sigma_g^+)+O_2^-(X^2\Pi_g)$ channel. Photodissociation producing $O_2(a^1\Delta_g)+O_2^-(X^2\Pi_g)$ at 349.0 nm yields a much higher degree of internal excitation than at 523.6 nm. The assignment of peaks II and III to the $O_2(b^1\Sigma_g^+)+O_2^-(X^2\Pi_g)$ channel are plausible but by no means definitive. With this assignment it appears that the $O_2(b^1\Sigma_g^+)+O_2^-(X^2\Pi_g)$ channel shows evidence for both low and high internal excitation pathways.

The 261.8 nm $P(E_T)$ in the top frame of Fig. 9 shows no identifiable structure. The $P(E_T)$ has a broad peak centered at 2.20 eV. This peak is 0.47 eV below below the maximum translational energy for the $O_2(b^1\Sigma_g^+)+O_2^-(X^2\Pi_g)$ channel (C, 2.67 eV). Thus the $O_2(b^1\Sigma_g^+)+O_2^-(X^2\Pi_g)$ channel at 261.8 nm shows only a high internal excitation pathway.

V. DISCUSSION

The measured photofragment energy and angular distributions indicate that photodestruction of O_4^- is complicated and proceeds through multiple photodissociation *and* dissociative photodetachment channels. The complexity of the spectra are not surprising considering the number of low-lying O_2 states. The strongly anisotropic photofragment distributions observed at the three wavelengths indicate that both photodissociation and dissociative photodetachment occur rapidly. Since rotational motion of the photoexcited complex reduces photofragment anisotropy,[41] photodissociation (with $\beta\approx 2$) must be occurring faster than the $\sim$1 to 10-ps time scale of molecular rotation.

The translational energy release features assigned to photodissociation (as opposed to dissociative photodetachment, in which a free electron is also produced) provide a direct determination of the partitioning of energy between translational and internal degrees of freedom. These measurements lead to plausible assignments for product electronic states and an independent verification of the O_2^-–O_2 bond energy. The assignment of the lowest energy photodissociation channel to $O_2(a^1\Delta_g)+O_2^-(X^2\Pi_g)$ indicates that the ground electronic state of the parent O_4^- is a doublet, not a quartet. Although doublet ground state O_4^- could produce $O_2(X^3\Sigma_g^-)+O_2^-(X^2\Pi_g)$ products in a spin-allowed dissociation, this channel is not observed. Johnson and co-workers[14] have also found little evidence for photodestruction at 1064 nm, suggesting that photodissociation to ground state products does not occur at that wavelength either.

The nearly complete partitioning of the available energy into product translation in the $O_2(a^1\Delta_g)+O_2^-(X^2\Pi_g)$ photodissociation channel at 523.6 nm is interesting. A small amount of $O_2^-(v=1)$ is observed in the photodissociation $P(E_T)$ at this wavelength, but the dominant (86%) channel is assigned to $O_2(v=0)+O_2^-(v=0)$ products. In addition, the sharp peak at 0.80 eV indicates that a narrow range of rotational states in the two diatomic products are excited. This implies that the structure of O_4^- is characterized by a well-defined geometry, and the dissociation occurs with a well-defined exit-channel impact parameter. An impulse model[42,43] can be used to predict the partitioning of the maximum available energy between translation and internal degrees of freedom. Using the structure inferred from matrix isolation[20] and theoretical studies[23] (C_{2h} symmetry, $r_{O-O}=1.26$ Å in the O_2 moieties, $\theta_{OOO}=110°$), this model predicts an energy of 0.41 eV in rotation and 0.05 eV in vibration. This degree of rotational excitation is much higher than the observed offset of the peak at $E_T=0.80$ eV from $E_{T,MAX}=0.93$ eV calculated using Hiraoka's bond energy.[11] Thus the impulsive model using the matrix structure fails to explain the rotational distribution implicit in the peak width observed at 523.6 nm. Due to the large O–O–O bond angle, the impulse model predicts little vibrational excitation, consistent with experiment. However, r_{O-O} is expected to change from 1.26 Å in O_4^- to $r_e=1.216$ and 1.35 Å in $O_2(a^1\Delta_g)$ and $O_2^-(X^2\Pi_g)$, respectively.[38] In this case a Franck–Condon distribution of product vibrations in O_2 and O_2^- might be expected. Given the large change in bond lengths, such a distribution would be characterized by significant vibrational excitation. In fact, very little vibrational excitation is observed at 523.6 nm, indicating that a Franck–Condon model for the vibrational distribution is not applicable. Thus both impulsive and Franck–Condon models for the energy partitioning in photodissociation at 523.6 nm fail.

At 349.0 and 261.8 nm the $P(E_T)$ are characterized by a greater partitioning of energy into internal (rotational, vibrational, and electronic) degrees of freedom. The fact that resolved vibrational features are not observed indicates that more rotational excitation is occurring at these wavelengths. The simple impulse model predicts the rotational excitation to increase significantly at 349.0 and 261.8 nm, however, the amount of rotational energy is far higher than observed. Dissociation feature II (see Fig. 9) observed at 349.0 nm and assigned to the $O_2(b^1\Sigma_g^+)+O_2^-(X^2\Pi_g)$ channel is interesting, as the peak of this feature is only 0.16 eV below the maximum available energy for this dissociation channel. Thus the energy partitioning in this case is very similar to that observed in the $O_2(a^1\Delta_g)+O_2^-(X^2\Pi_g)$ photodissociation channel at 523.6 nm. Features I and III at 349.0 nm and the 261.8 nm $P(E_T)$, however, have peaks occurring an average of 0.45 eV below the respective thresholds. This raises the possibility that there are at least two different dissociative states correlating to each of these asymptotes which are characterized by different geometries and hence different energy partitioning. The excited state dynamics of O_4^- photodissociation are complex and inviting to further study.

A question that remains unanswered is whether the excess electron in O_4^- is in a delocalized molecular orbital or is shared via a vibronic interaction between two instantaneously distinguishable O_2 moieties. Comita and Brauman studied the photodissociation cross section of the dimer anion of toluquinone,[3] and observed vibronic structure attributed to resonant charge transfer between the two monomers below the photodetachment threshold. They applied a vibronic coupling model of resonant charge transfer[44,45] to analyze the structure in the photodestruction cross section. This analysis indicated that for the dimer anion of toluquinone, the electron is highly localized and the structure is consistent

with a solvated monomer anion. While we have not been able to perform a similar measurement of the photodissociation cross section for O_4^-, the influence of a solvated anion structure on the photodissociation dynamics can be considered. If the excess charge is localized on one of the O_2 moieties and resonant charge transfer is optically promoted, subsequent vibronic interactions could lead to production of O_2 and O_2^- closer to their asymptotic equilibrium bond lengths. This would yield little product vibrational excitation, as observed at 523.6 nm. The vibronic coupling treatments presented to date involve only the ground state and a single excited state. The photodissociation of O_4^- always occurs to electronically excited products, however, requiring a generalization of the vibronic coupling model to include several excited states.

The product angular distributions observed from the photodissociation of O_4^- are characterized by an anisotropy parameter near the parallel limit of 2.0, indicating that the transition moment for photodissociation lies directly along the breaking $O_2^- - O_2$ bond. In a one-electron transition, charge transfer between the O_2 moieties necessarily involves motion of the electron along an $O_2 - O_2$ coordinate. It is possible that the parallel photofragment angular distribution is a consequence of photodissociation proceeding by charge transfer between the O_2 species followed by rapid dissociation. It is interesting to note that the $(SO_2)_2^-$ anion also exhibits competing photodissociation and photodetachment pathways.[4,46] Photodissociation in this dimer anion was observed to occur by a parallel transition ($\beta \sim 1.0$) by Bowers and co-workers.[46] Measuring photofragment angular distributions of other dimer anions will be of interest to evaluate whether or not this is a general phenomenon.

The photochemistry of O_4^- is complicated by the fact that dissociative photodetachment is the dominant photodestruction pathway at all of the wavelengths studied in this work. A theoretical description of the interaction between the dissociative photodetachment continuum and the photodissociation continuum remains to be given. Determination of the branching ratio between dissociative photodetachment and photodissociation is also obscured by autodetachment of vibrationally and/or electronically excited states of O_2^- after photodissociation.

VI. CONCLUSIONS

In conclusion, these experiments have shown that both photodissociation and dissociative photodetachment of O_4^- occur at 523.6, 349.0, and 261.8 nm. The lowest energy photodissociation channel observed is assigned to $O_2(a^1\Delta_g) + O_2^-(X^2\Pi_g)$, indicating that the ground state of O_4^- is a doublet. At all wavelengths photodissociation occurs by a parallel electronic transition. At 523.6 nm, photodissociation primarily yields $v=0$ diatomic products with little rotational excitation. The observed rotational excitation is not consistent with a simple impulse model based on the structure of O_4^- determined in matrix-isolation studies. At higher photon energies, the nature of the energy partitioning changes, with evidence for both low and high internal excitation pathways observed. The lack of vibrational excitation at 523.6 nm indicates that a Franck–Condon model of the vibrational excitation, based on a symmetric O_4^- structure, fails. An alternative view of the bonding in O_4^- by vibronic charge transfer interactions between O_2 and O_2^- may provide a reasonable explanation of the observed energy partitioning and photofragment angular distributions.

Theoretical studies on the structure of O_4^- ground and excited electronic states will be of great use in the further interpretation of the results reported in this paper. Such calculations are anticipated to be difficult, however, as O_4^- is an open-shell weakly bound anion. Further studies of dissociative photodetachment, involving coincidence measurement of the photoelectron and photofragments, are ongoing[47] and should also reveal the extent to which autodetaching states of O_2^- produced in photodissociation play a role in the photodestruction dynamics of O_4^-. We hope to extend studies of photodissociation and dissociative photodetachment to other small dimer anions, such as $(SO_2)_2^-$ and $(CO_2)_2^-$, in the near future. These studies should provide a clearer picture of the structure and dynamics of dimer anions.

ACKNOWLEDGMENTS

This work was supported by the Chemistry Division of the National Science Foundation. REC acknowledges support from a Camille and Henry Dreyfus New Faculty Award and a 1994 Packard Fellowship in Science and Engineering. Melissa Castle, Anthony Mrse, and Scott Graybeal are acknowledged for their efforts on apparatus construction.

[1] J. M. Farrar, in *Cluster Ions*, edited by T. Baer, C. Y. Ng, and I. Powis (Wiley, New York, 1993), pp. 243–317.
[2] M. J. DeLuca, C. C. Han, and M. A. Johnson, J. Chem. Phys. **93**, 268 (1990).
[3] P. B. Comita and J. I. Brauman, J. Am. Chem. Soc. **109**, 7591 (1987).
[4] S. T. Arnold, J. G. Eaton, D. Patel-Misra, H. W. Sarkas, and K. H. Bowen, in *Ion and Cluster Ion Spectroscopy and Structure*, edited by J. P. Maier (Elsevier, New York, 1989), pp. 417–472.
[5] L. C. Lee and G. P. Smith, J. Chem. Phys. **70**, 1727 (1979).
[6] P. C. Cosby, R. A. Bennett, J. R. Peterson, and J. T. Moseley, J. Chem. Phys. **63**, 1612 (1975).
[7] P. C. Cosby, J. H. Ling, J. R. Peterson, and J. T. Moseley, J. Chem. Phys. **65**, 5267 (1976).
[8] G. P. Smith, L. C. Lee, P. C. Cosby, J. R. Peterson, and J. T. Moseley, J. Chem. Phys. **68**, 3818 (1978).
[9] L. C. Lee and G. P. Smith, J. Chem. Phys. **70**, 1727 (1979).
[10] D. C. Conway and L. E. Nesbitt, J. Chem. Phys. **48**, 509 (1968).
[11] K. Hiraoka, J. Phys. Chem. **89**, 3190 (1988).
[12] C. C. Han and M. A. Johnson, Chem. Phys. Lett. **189**, 460 (1992).
[13] L. A. Posey, M. J. Deluca, and M. A. Johnson, Chem. Phys. Lett. **131**, 170 (1986).
[14] M. J. DeLuca, C. C. Han, and M. A. Johnson, J. Chem. Phys. **93**, 268 (1990).
[15] R. J. Celotta, R. A. Bennett, J. L. Hall, M. W. Siegel, and J. Levine, Phys Rev. A **6**, 631 (1972).
[16] C. C. Han and M. A. Johnson, Chem. Phys. Lett. **189**, 460 (1992).
[17] C. R. Sherwood, M. C. Garner, K. A. Hanold, K. M. Strong, and R. E. Continetti, J. Chem. Phys. **102**, 6949 (1995).
[18] R. E. Continetti, C. R. Sherwood, M. C. Garner, K. A. Hanold, and K. M. Strong, SPIE Conference on Laser Techniques for State-Selected and State-to-State Chemistry III, Vol. 2548, 122 (1995).
[19] K. A. Hanold, C. R. Sherwood, and R. E. Continetti, J. Chem. Phys. **103**, 9876 (1995).

[20] L. Manceron, A-M. Le Quere, and J-P. Perchard, J. Phys. Chem. **93**, 2960 (1989).
[21] W. E. Thompson and M. E. Jacox, J. Chem. Phys. **91**, 3826 (1989).
[22] D. M. Lindsay, D. R. Herschbach, and A. L. Kwiram, J. Phys. Chem. **87**, 2113 (1983).
[23] D. C. Conway, J. Chem Phys. **50**, 3864 (1969).
[24] K. Ohta and K. Morokuma, J. Phys. Chem. **91**, 401 (1987).
[25] X. Y. Li, A. M. Tian, F. C. He, and G. S. Yan, Chem. Phys. Lett. **233**, 227 (1995).
[26] The photoelectron spectrometer, not used in the present work, is described in K. A. Hanold, C. R. Sherwood, M. C. Garner, and R. E. Continetti, Rev. Sci. Instrum. **66**, 5507 (1995).
[27] M. C. Garner, C. R. Sherwood, K. A. Hanold, and R. E. Continetti, Chem. Phys. Lett. **248**, 20 (1996).
[28] R. E. Continetti, D. R. Cyr, D. L. Osborn, D. J. Leahy, and D. M. Neumark, J. Chem. Phys. **99**, 2616 (1993).
[29] M. A. Johnson and W. C. Lineberger, in *Techniques in Chemistry*, edited by J. M. Farrar and W. H. Saunders (Wiley, New York, 1988), Vol. 20, p. 591.
[30] J. M. B. Bakker, J. Phys. E **6**, 785 (1973); **7**, 364 (1974).
[31] L. D. Gardner, M. M. Graff, and J. L. Kohl, Rev. Sci Instrum. **57**, 177 (1986).
[32] D. P. DeBruijn and J. Los, Rev. Sci. Instrum. **53**, 1020 (1982).
[33] D. J. Lavrich, M. A. Buntine, D. Serxner, and M. A. Johnson, J. Chem. Phys. **99**, 5910 (1993).
[34] S. Kornig, J. H. Beijersbergen, W. J. Van der Zande, and J. Los, Int. J. Mass Spectrom. Ion Proc. **93**, 49 (1989).
[35] R. N. Zare, Mol. Photochem. **4**, 1 (1972).
[36] C. R. Sherwood, Ph.D. thesis, University of California, San Diego, 1995.
[37] P. C. Cosby and D. L. Huestis, J. Chem. Phys. **97**, 6109 (1992); D. M. Neumark, K. R. Lykke, T. Anderson, and W. C. Lineberger, Phys. Rev. A **32**, 1890 (1985); M. J. Travers, D. C. Cowles, and G. B. Ellison, Chem. Phys. Lett. **164**, 449 (1989).
[38] K. P. Huber and G. Herzberg, *Molecular Spectra and Molecular Structure IV. Constants of Diatomic Molecules* (Van Nostrand, New York, 1979), pp. 491–507.
[39] G. Herzberg, *Molecular Spectra and Molecular Structure I. Spectra of Diatomic Molecules* (Van Nostrand, New York, 1950), pp. 319.
[40] Y. Hatano, *Electronic and Atomic Collisions*, edited by D. C. Lorents, W. E. Meyerhof and J. R. Peterson (Elsevier, New York, 1986), pp. 153–173.
[41] S.-C. Yang and R. Bersohn, J. Chem. Phys. **61**, 4400 (1974).
[42] G. E. Busch and K. R. Wilson, J. Chem. Phys. **56**, 3626 (1972).
[43] K. A. Trentelman, S. H. Kable, D. B. Moss, and P. L. Houston, J. Chem. Phys. **91**, 7498 (1989).
[44] J. McHale and J. Simons, J. Chem. Phys. **72**, 425 (1979).
[45] K. Y. Wong and P. N. Schatz, Prog. Inorg. Chem. **28**, 369 (1982).
[46] H.-S. Kim and M. T. Bowers, J. Chem. Phys. **85**, 2178 (1986).
[47] K. A. Hanold, M. C. Garner, and R. E. Continetti, Phys. Rev. Lett. **77**, 3335 (1996).